



Synthesis and Microwave Absorbing Properties of Porous One-Dimensional Nickel Sulfide Nanostructures

Min Lu¹, Qian Wu¹, Xiao-Hui Guan¹, Wei Xu², Hao-Yue Zhang², Xin Di³, Guang-Sheng Wang^{2*} and Shao-Hua Dong^{3*}

¹ School of Chemical Engineering, Northeast Electric Power University, Jilin, China, ² School of Chemistry, Beihang University, Beijing, China, ³ Pipeline Technology Research Center, China University of Petroleum–Beijing, Beijing, China

OPEN ACCESS

Edited by:

Wenbo Wang,
Lanzhou Institute of Chemical Physics
(CAS), China

Reviewed by:

Zheng Ren,
University of Connecticut,
United States
Aiwei Tang,
Beijing Jiaotong University, China

*Correspondence:

Guang-Sheng Wang
wanggsh@buaa.edu.cn
Shao-Hua Dong
shdong@cup.edu.cn

Specialty section:

This article was submitted to
Green and Sustainable Chemistry,
a section of the journal
Frontiers in Chemistry

Received: 30 June 2018

Accepted: 20 August 2018

Published: 11 October 2018

Citation:

Lu M, Wu Q, Guan X-H, Xu W,
Zhang H-Y, Di X, Wang G-S and
Dong S-H (2018) Synthesis and
Microwave Absorbing Properties of
Porous One-Dimensional Nickel
Sulfide Nanostructures.
Front. Chem. 6:405.
doi: 10.3389/fchem.2018.00405

One-dimensional (1D) porous Ni_xS_y nanostructures have been successfully fabricated by two-step method consisting of solvothermal and subsequent annealing process. The suitable heat treatment temperature and reaction time play crucial roles in the final structure, morphology, as well as performance. The uniform and perfect porous Ni_xS_y nanostructures obtained at 310°C exhibit outstanding microwave absorption performances. A minimum reflection loss of −35.6 dB is achieved at 8.5 GHz, and the effective absorption bandwidth almost covers 14.5 GHz with the absorber thickness range of 2.0–5.0 mm. It can be supposed that this porous structure with rough surface which is favor for increasing the microwave multiple reflection and scattering, contributes a high-performance electromagnetic absorption.

Keywords: porous, nickel sulfide, one-dimensional, dielectric loss, microwave absorption

INTRODUCTION

Microwave absorber with strong capacity in absorption, low proportion in filler loading, thin thickness in coating, and wide bandwidth in absorption frequency, has aroused burgeoning research interest because of their great potential applications both in military and civil fields, including stealth technology, information security, electromagnetic interference shielding, and healthcare (Zhu et al., 2010; Zhao H. et al., 2014). As is well known that many factors such as morphology, geometry and structure, have vital impacts on determining the microwave absorption (MA) properties (He et al., 2013). Conventional microwave absorbers with different morphologies that have been divided into three classes are as follows: (1) one-dimensional nanostructures such as ZnO nanowires (Wang et al., 2014), Bi₃S₂ nanorods (Luo et al., 2014); (2) two-dimensional materials such as MoS₂ nanosheets (Ning et al., 2015), α-Fe₂O₃ flakes (Lv et al., 2015a); and (3) three-dimensional network structures, including Co₂₀Ni₈₀ hierarchical nanospheres (Liu et al., 2015), Ni chains nets (Liu et al., 2016), Fe₃O₄@carbon ordered arrays (Yuan et al., 2015) and so on. However, the aforementioned materials usually possess high density, thus leading to severe limitations to their practical applications in some specialized fields. In this regard, materials with characteristics of low density and special void spaces, such as yolk-shell structural microspheres (Liu et al., 2013; Yu et al., 2014; Qiang et al., 2016), foam composites (Zhang Y. et al., 2015; Zhao H. B. et al., 2016), as well as porous nanostructures (Yan et al., 2009; Zhou et al., 2010; Zhu et al., 2011), are highly beneficial to obtaining superior microwave absorption performance.

Considerable attention has been concentrated on the porous structure of MA materials owing to its fascinating characteristics. For example, Liu et al. fabricated porous carbon/Co composites, and the results suggested that the composites with large dielectric loss could achieve a minimum RL of -40 dB at 4.2 GHz with a coating thickness of 5 mm (Liu et al., 2008). Lv et al. synthesized Co/CoO porous 3-D flower nanostructure through annealing process at 400°C and found that the minimal reflection loss was up to -50 dB when the coating thickness was 3.5 mm (Lv et al., 2015b). Similarly, Wang et al. reported the formation of porous flower-like NiO decorated graphene, and the composites with a filler loading of 25 wt% exhibited highly MA performance (-59.6 dB) because of their special porous structures and numerous void spaces (Wang et al., 2017). Benefiting from the porous structure, the above-mentioned materials show superior electromagnetic wave absorption performance, which reveals that these porous materials are effective as MA materials.

Metal sulfides, as semiconductor materials, have been proven to have promising potential as an ideal microwave absorber on account of their typical dielectric loss mechanism (Zhang X. J. et al., 2017). Recent studies have suggested that metal sulfides including MoS_2 (Wang et al., 2015), CoS_2 (Zhang C. et al., 2017), CdS (Zhang et al., 2014), and CuS (He et al., 2014), as well as various phase of nickel sulfides (Zhou et al., 2010) can effectively absorb electromagnetic waves and attenuate them in the form of thermal energy. However, the microwave-absorbing properties of Ni_xS_y with special porous structure have not been reported previously. Based on the above study, we demonstrated the successful design and fabrication of porous one-dimensional Ni_xS_y nanomaterial through a facile solvothermal route together with annealing process. The MA properties of resultant composites were investigated in detail for the first time. As expected, the synthesized Ni_xS_y nanostructure exhibited excellent microwave absorption property confirming that this material can be used as high-performance microwave absorber.

MATERIALS AND METHODS

Preparation of Porous Ni_xS_y

Nickel nitrate hexahydrate ($\text{Ni}(\text{NO}_3)_2 \cdot 6\text{H}_2\text{O}$), elemental sulfur, ethylene glycol (EG), and ethylenediamine (EN) were purchased from Nanjing Chemical Reagent Co. All of the chemical reagents were analytical-grade purity and used without further purification.

Typically, nickel sulfide was synthesized by the reaction of $\text{Ni}(\text{NO}_3)_2 \cdot 6\text{H}_2\text{O}$, EN and sulfur powder in EG. At first, $\text{Ni}(\text{NO}_3)_2 \cdot 6\text{H}_2\text{O}$ (0.3489 g) was added to EG (135 mL) under strong magnetic stirring to form a light green homogeneous solution. Then the sulfur powder (0.0288 g) was dissolved in EN (15 mL) through ultrasonic treatment. Mix the two solutions together and put it into oil bath, maintained at 120°C for 6 h. After being cooled to room temperature, the resulting solid precursors were centrifuged, washed with alcohol to remove possible remnant, and finally dried in air at 60°C for 24 h. The dried precursors were treated at 310°C for 2 h with a heating rate of $2^\circ\text{C}/\text{min}$ under N_2 atmosphere to get the final Ni_xS_y products.

Preparation of Nickel Sulfide/PVDF Nanocomposites

The polyvinylidene fluoride (PVDF) was first dispersed in *N,N*-dimethylformamide (20 mL) under magnetic stirring for 1 h. Then, the desired amount of nickel sulfide was added into the suspension. After ultrasonication for another 1 h, the mixture was poured onto a glass plate and dried at 80°C for 24 h. The samples for testing were also compacted into a cylindrical compact ($\Phi_{out} = 7.00$ mm and $\Phi_{in} = 3.04$ mm) by hot pressing at 210°C under 5 MPa (pressed for 15 min, followed by cooling to room temperature under the same pressure).

Instrumental Analyses

The X-ray diffraction (XRD) pattern of the nickel sulfide product was carried out on a Rigaku, Dmax2200 diffractometer equipped with a CuK α radiation source ($\lambda = 1.5416$ Å) in the range of $2\theta = 10$ – 80° . For the phase analysis. Further microstructural analyses were performed by using a FEI Quanta 250 field emission gun environmental scanning electron microscope (JSM-6700F microscope) at 15 kV. In brief, SEM samples were prepared by diluting the final products with alcohol by ultrasonic treatment and dropping it on the silicon slice. The relative permittivity (ϵ' , ϵ'') and permeability (μ' , μ'') values were measured using two-port vector network analyzer (Agilent E5071C) over the frequency of 2 – 18 GHz at room temperature, coupled with a coaxial wire setup. Finally, the reflection loss (RL, dB) value which presents the ratio of the total reflected microwave power against the incident microwave power can be calculated by using the following formulas (Abbas et al., 2006; Xu et al., 2018).

$$Z_{in} = \sqrt{\frac{\mu_r}{\epsilon_r}} \tanh \left[j \left(\frac{2f\pi d}{c} \right) \sqrt{\mu_r \epsilon_r} \right] \quad (1)$$

$$RL(\text{dB}) = 20 \log \left| \frac{Z_{in} - 1}{Z_{in} + 1} \right| \quad (2)$$

where Z_{in} is the normalized input characteristic impedance, f is the frequency of microwave, d is the thickness of the absorber. A lower RL value stands for a better MA performance.

RESULTS AND DISCUSSION

An illustration of the synthesis of the Ni_xS_y is shown in **Figure S1**. We first prepared the precursors of Ni_xS_y nanorods by a simple solvothermal method in a controlled way as described later. Then the collected dried precursors were transferred into a tube furnace and annealed at 310°C for 2 h under an N_2 atmosphere, which eventually led to the generation of the porous Ni_xS_y . It is well recognized that reaction parameters such as temperature, pressure, reaction time, type of solvent, and concentration of reagents, have a huge effect on the morphology of the products. In the present reaction system, Ethylene glycol and Ethylenediamine were applied as solvents for the precursors synthesis of Ni_xS_y , and the temperature as well as reaction time was tightly regulated so that the precursors at a well-defined state were obtained.

Figure 1 shows the representative SEM images of the precursors prepared at different temperature of 80 , 100 , 120 , 140 ,

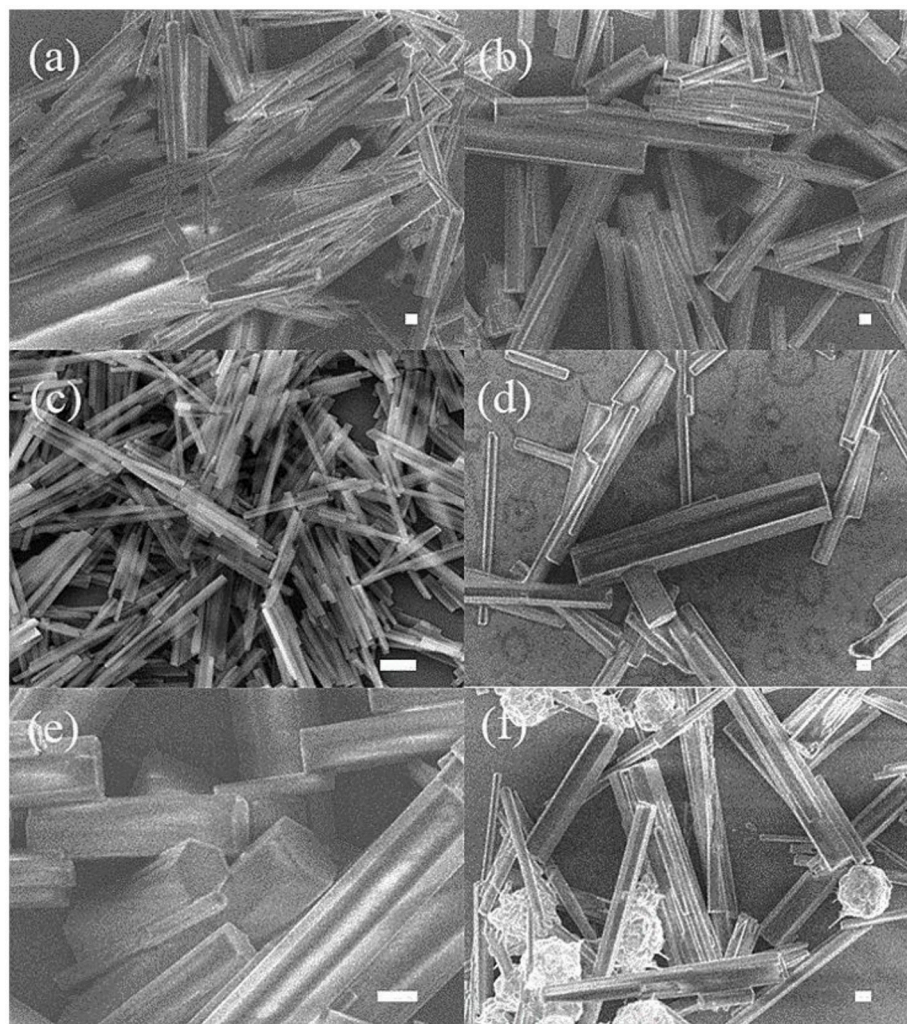


FIGURE 1 | SEM images of precursor of Ni_xS_y samples under different reaction temperatures: (a) 80, (b) 100, (c) 120, (d) 140, (e) 160, and (f) 180°C. (scale bar = 1 μm).

160, and 180°C, respectively. When the reaction is performed under the lower temperature (80 and 100°C), although one-dimensional structures of products can be formed, their thicknesses and lengths are varying greatly. On the contrary, when the temperature reaches 180°C, the 1D nanostructures are nonuniform, and a certain number of spherical impurities emerge. By comparing the morphology of the products under different temperature conditions, the best reaction temperature is determined. The products are well-defined nanorods with diameters of about 50 nm and lengths of several micrometers at the suitable reaction temperature of 120°C (**Figure 1c**). On the other hand, the stages of the growth process are monitored at 120°C by varying the reaction time from 2 to 10 h (**Figure S2**). It is interesting to find that reaction time does not change the overall morphology of the precursors. However, the yield of the products is very low within a short period of 2 h, indicating the slow reaction rate in such reaction system. Further increasing

the reaction time produce more products, while the diameter and structure of the nanorods remain stable.

To obtain porous 1D nanostructures, the precursors were annealed at different temperatures ranging from 280 to 330°C under the flowing nitrogen gas, and the final products are exhibited in **Figure 2**. It can be seen that the surfaces are actually becoming porous with annealing temperature, and the as-obtained Ni_xS_y retain the rods morphology with appropriate porosity when prepared at 310°C. Further increasing the annealing temperature will led to 1D structural instability and collapse. The energy-dispersive X-ray spectroscopy (EDS) indicates that the obtained product is composed of Ni, S, C, N, and O elements, also demonstrating a very homogeneous elemental distribution (**Figure 3**). It is worth mentioning that the C, N, and O element signals originate from the incomplete decomposition of organic compositions of precursors during heat treatment. Meanwhile, the XRD results suggest that the

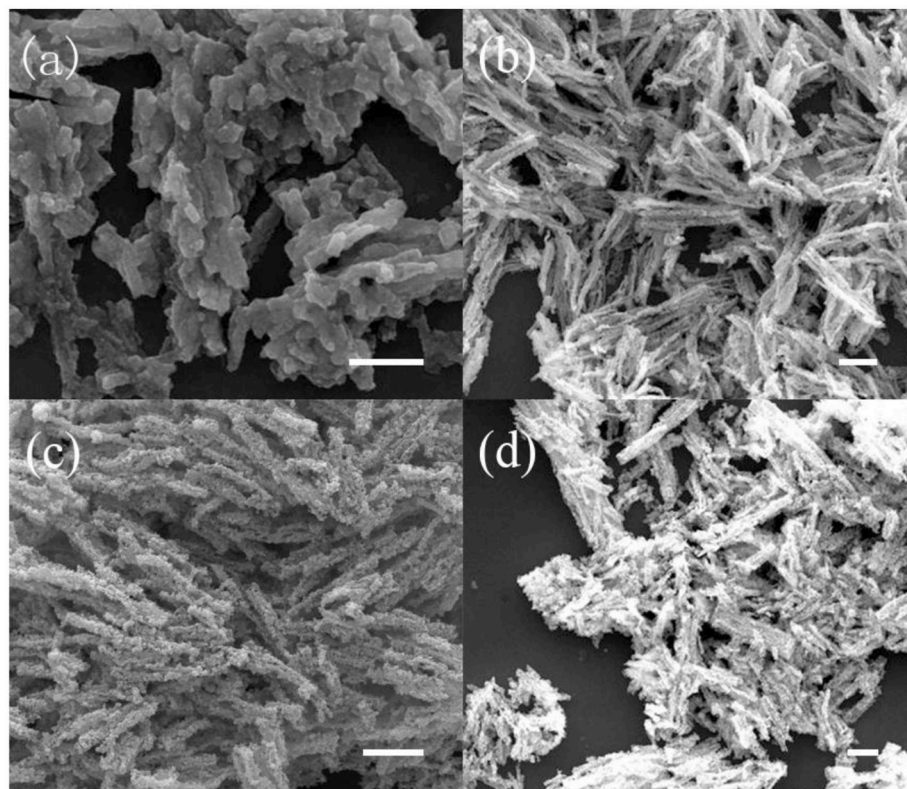


FIGURE 2 | SEM images of Ni_xS_y samples under different annealing temperatures: (a) 280, (b) 300, (c) 310, and (d) 330°C. (scale bar = 1 μm).

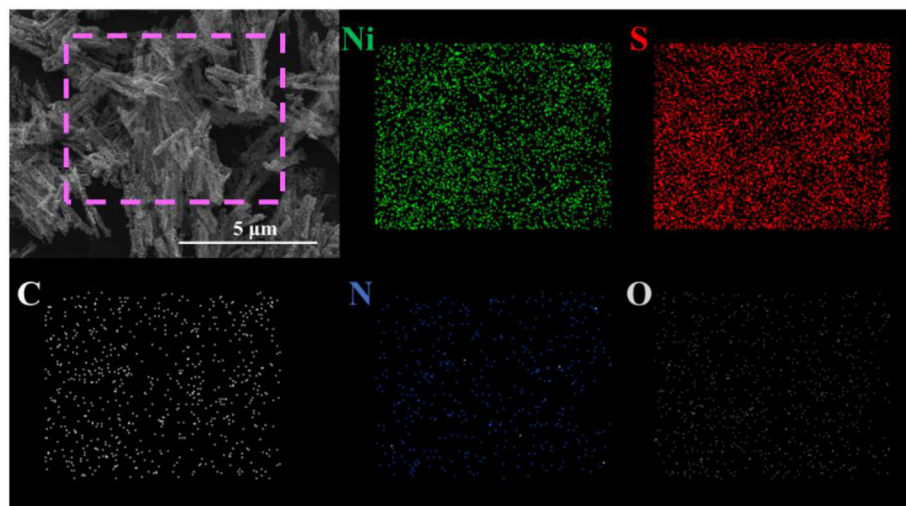


FIGURE 3 | FESEM image of the Ni_xS_y nanorods and corresponding elemental mapping images of Ni, S, C, N, and O.

as-synthesized products are poorly crystallized, containing NiS_2 phase and Ni_7S_6 phase (Figure S3).

Figures 4A,B show the frequency dependence of the real part (ϵ') and imaginary part (ϵ'') of the complex permittivity for $\text{Ni}_x\text{S}_y/\text{PVDF}$ composites with 10, 20, 30, and 40 wt% filler

loadings in the frequency range of 2–18 GHz. Generally, the ϵ' is known to stand the storage capability of electromagnetic energy, and ϵ'' associated with various of polarization present the energy dissipation (Zhang X. et al., 2015; Zhao B. et al., 2016). As can be seen in Figure 4, with the increase of Ni_xS_y , the ϵ'

and ϵ'' values show a similar tendency. For nanohybrids with low concentration of filler (10 and 20 wt%), the values of ϵ' and ϵ'' are approximately equal to some certain constant in the whole frequency range ($\epsilon' = 4$, $\epsilon'' = 0.5$, and $\epsilon' = 6$, $\epsilon'' = 1$). With the

Ni_xS_y proportion increasing from 20 to 30 wt%, the ϵ' increases from 6 to 13 and the ϵ'' changes from 1 to 4.5 at 2 GHz. However, when the proportion of fillers is increased to 40 wt%, both the ϵ' and ϵ'' dramatically decrease, which is possibly due to the

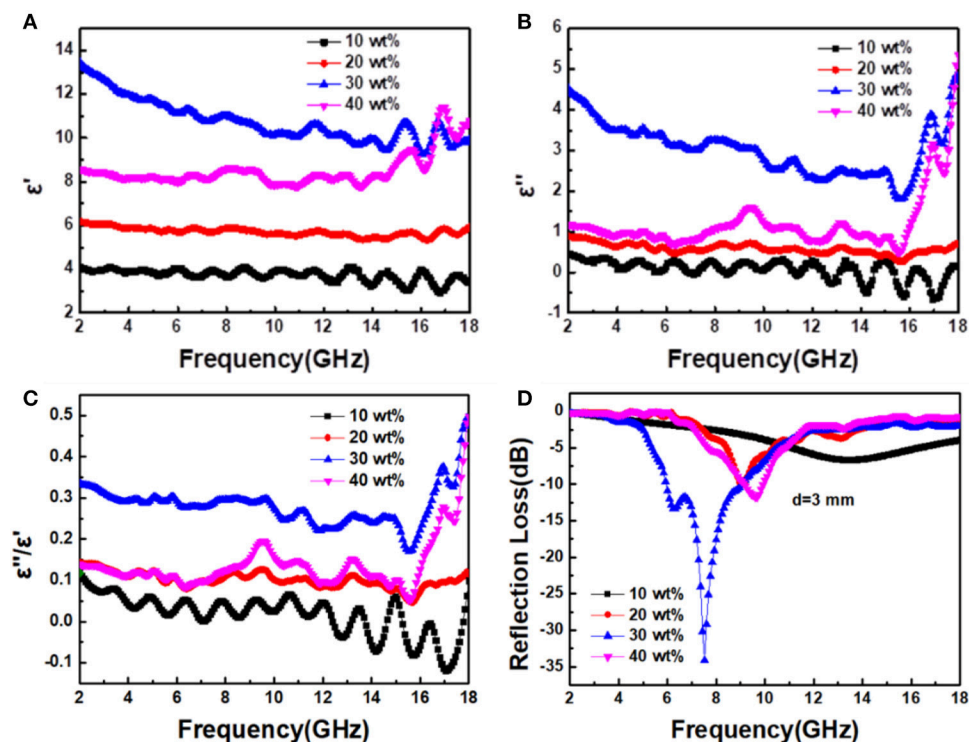


FIGURE 4 | Frequency dependence of (A) real part and (B) imaginary part of permittivity, (C) dielectric loss tangent, and (D) reflection loss under a 3 mm thickness for Ni_xS_y composites with different filler loadings.

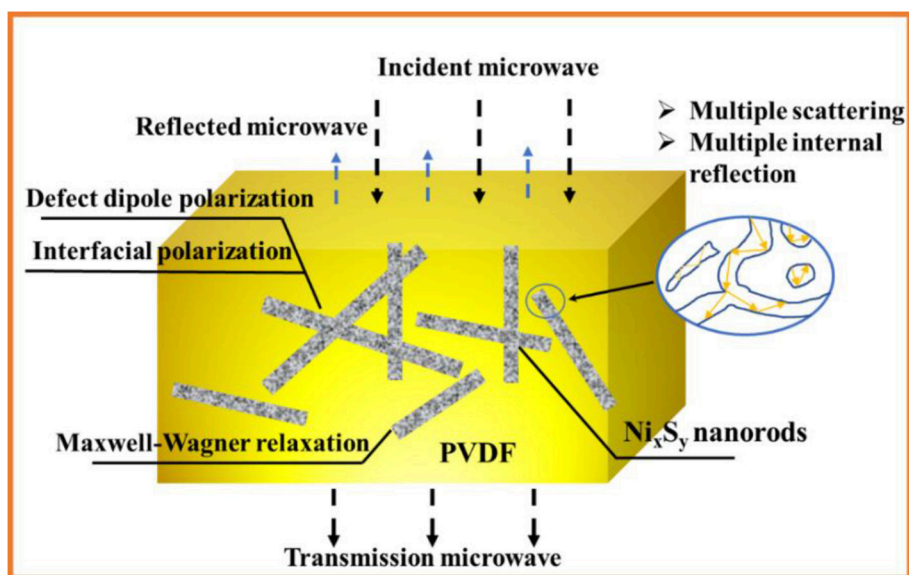


FIGURE 5 | Possible mechanisms of microwave absorption for porous Ni_xS_y /PVDF composites.

fact that the higher concentration of Ni_xS_y in this nanohybrid may result in severe agglomeration. Similar phenomena could be observed in dielectric loss tangent ($\tan \delta_e = \epsilon''/\epsilon'$) which is universally applied to evaluate the dielectric loss capacity of the microwave absorber (Yang et al., 2017), shown in **Figure 4C**. It can be seen that the dielectric loss tangent increases with the Ni_xS_y proportion first, getting a maximum value of 0.35 with 30 wt% Ni_xS_y , and then decreases to a value of 0.1.

On the basis of the above analysis, it can be deduced that the nanohybrids with 30 wt% Ni_xS_y possess the best microwave absorption properties which is highly consistent with the test results, shown in **Figure 4D**. The minimum RL reaches -34 dB at 7.5 GHz with a thickness of 3 mm, indicating that 99.9% of incident electromagnetic wave is attenuated. Since

Ni_xS_y is a typical semiconductive material, various polarization, and related relaxation resulting in a strong dielectric loss are the dominant mechanism for microwave attenuation (Zhao et al., 2015). The dielectric loss of Ni_xS_y mainly originate from the defect dipole polarization, the interfacial polarization, and the electronic relaxation loss. First, the defect dipoles are generated by the charge unbalance around the sulfur vacancies in the Ni_xS_y lattice, while the interfacial polarizations come from the existence of plentiful interfaces between porous fillers and polymer matrix. Moreover, the porous structures of fillers with rough surfaces further induce the multiple reflection and scattering, resulting in more longer propagation path and greater energy loss (**Figure 5**). Second, the carbonation of precursors benefits electrical conduction, while the internal

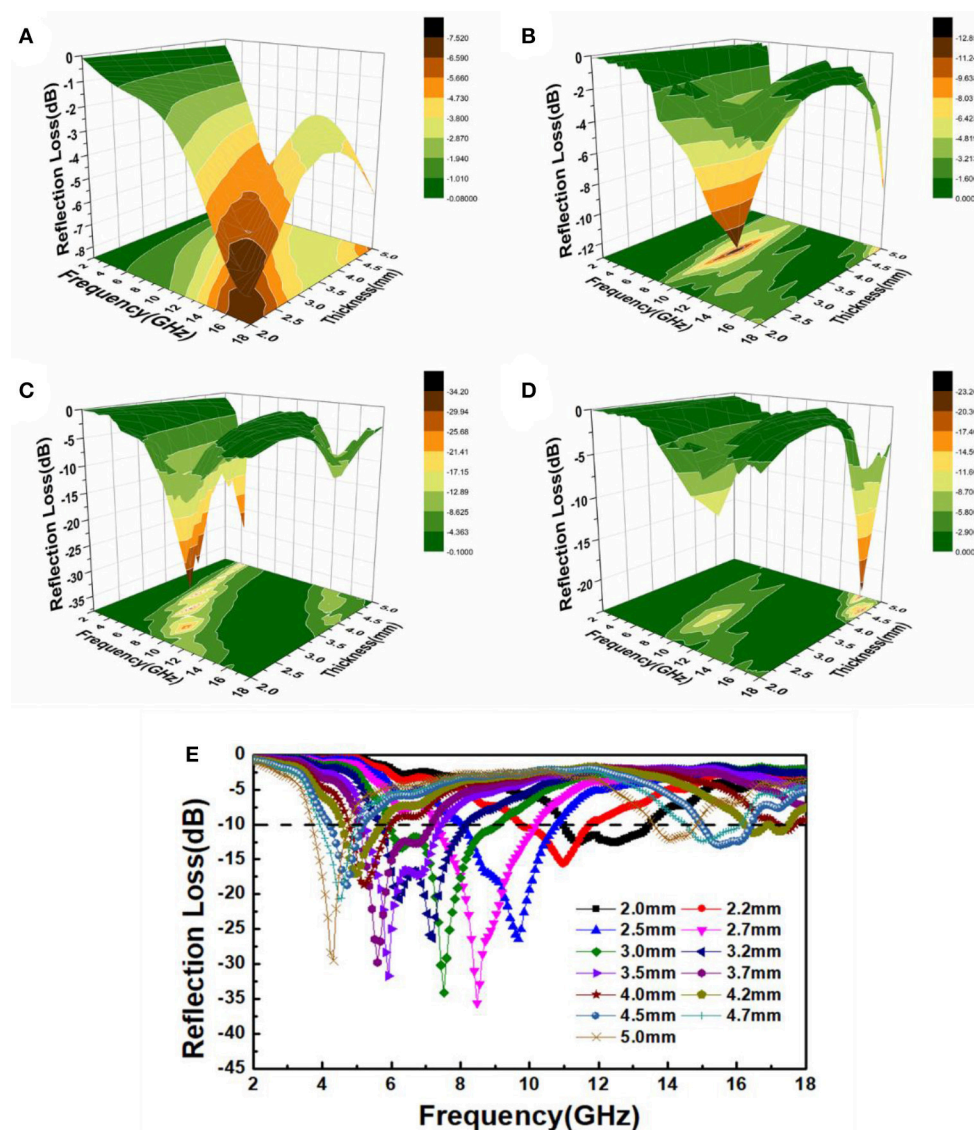


FIGURE 6 | Three-dimensional presentations of the reflection loss for the Ni_xS_y composites with different filler loadings: (A) 10, (B) 20, (C) 30, and (D) 40 wt%. (E) RL curves for 30 wt% Ni_xS_y composites with different thickness.

doping with nitrogen favors electron transport thus further improving electrical conduction. Furthermore, the calcination also induces a structural disorder and defects into Ni_xS_y that frequently lead to an enhanced electrical activity. This calcination process results in significant electronic relaxation polarization, which would enhance the dielectric loss obviously.

Figures 6A–D shows three-dimensional presentations of calculated reflection loss for the $\text{Ni}_x\text{S}_y/\text{PVDF}$ with different filler loadings. Clearly, the composite with 30 wt% Ni_xS_y has the best performance, and the RL values under different thickness are shown in **Figure 6E**. The minimal reflection loss of -35.6 dB is obtained at 8.5 GHz with a coating thickness of 2.7 mm and the effective bandwidth is about 3 GHz. Furthermore, the RLs exceeding -10 dB in the frequency range of 3.68–18 GHz are obtained for a variation in absorber thicknesses of 2.0–5.0 mm, demonstrating that this kind of materials has great potential for use as a microwave absorber. Meanwhile, there is an interesting phenomenon that with the increasing thickness of absorber the RL peaks shift to the lower-region frequency. This phenomenon is consistent with a so-called quarter-wavelength ($\lambda/4$) matching model (Deng and Han, 2007; Wang et al., 2011, 2013) which plays another significant role in electromagnetic attenuation. The model can be expressed as $t_m = n\lambda/4 = nc/4f_m\sqrt{|\mu_r||\varepsilon_r|}$ ($n = 1, 3, 5$), where $|\mu_r|$ and $|\varepsilon_r|$ are the moduli of μ_r and ε_r , respectively. Besides, when the thickness of absorber satisfies above equation, the curves corresponding to wavelengths of $\lambda/4$ (crescent shape) can be observed (seen in **Figure 6C**).

CONCLUSIONS

In summary, we have successfully demonstrated an approach for the large-scale production of 1D porous Ni_xS_y nanostructures via solvothermal synthesis together with an annealing process.

REFERENCES

- Abbas, S. M., Chandra, M., Verma, A., Chatterjee, R., and Goel, T. C. (2006). Complex permittivity and microwave absorption properties of a composite dielectric absorber. *Compos. A Appl. Sci. Manufact.* 37, 2148–2154. doi: 10.1016/j.compositesa.2005.11.006
- Deng, L. J., and Han, M. G. (2007). Microwave absorbing performances of multiwalled carbon nanotube composites with negative permeability. *Appl. Phys. Lett.* 91:023119. doi: 10.1063/1.2755875
- He, S., Lu, C., Wang, G. S., Wang, J. W., Guo, H. Y., and Guo, L. (2014). Synthesis and growth mechanism of white-fungus-like nickel sulfide microspheres and their application in polymer composites with enhanced microwave-absorption properties. *ChemPlusChem* 79, 569–576. doi: 10.1002/cplu.201300435
- He, S., Wang, G. S., Lu, C., Liu, J., Wen, B., Liu, H., et al. (2013). Enhanced wave absorption of nanocomposites based on the synthesized complex symmetrical CuS nanostructure and poly(vinylidene fluoride). *J. Mater. Chem. A* 1, 4685–4692. doi: 10.1039/c3ta00072a
- Liu, J., Cao, M. S., Luo, Q., Shi, H. L., Wang, W. Z., and Yuan, J. (2016). Electromagnetic property and tunable microwave absorption of 3D nets from nickel chains at elevated temperature. *ACS Appl. Mater. Interfaces* 8, 22615–22622. doi: 10.1021/acsami.6b05480
- Liu, J., Xu, J., Che, R., Chen, H., Liu, M., and Liu, Z. (2013). Hierarchical $\text{Fe}_3\text{O}_4/\text{TiO}_2$ yolk-shell microspheres with enhanced microwave-absorption properties. *Chem. A Eur. J.* 19, 6746–6752. doi: 10.1002/chem.201203557
- Liu, Q., Xu, X., Xia, W., Che, R., Chen, C., Cao, Q., et al. (2015). Dependency of magnetic microwave absorption on surface architecture of $\text{Co}_2\text{O}_3/\text{Ni}_8\text{O}$ hierarchical structures studied by electron holography. *Nanoscale* 7, 1736–1743. doi: 10.1039/c4nr05547k
- Liu, Q. L., Zhang, D., and Fan, T. X. (2008). Electromagnetic wave absorption properties of porous carbon/Co nanocomposites. *Appl. Phys. Lett.* 93:013110. doi: 10.1063/1.2957035
- Luo, X., Wang, G. S., Guo, H. Y., Zhang, X. J., Cao, W. Q., Wei, Y. Z., et al. (2014). Enhanced wave-absorption properties of nanocomposites based on the synthesized Bi_2S_3 nanorods and polyvinylidene fluoride. *ChemPlusChem* 79, 1089–1095. doi: 10.1002/cplu.201402050
- Lv, H., Liang, X., Cheng, Y., Zhang, H., Tang, D., Zhang, B., et al. (2015a). Coin-like $\alpha\text{-Fe}_2\text{O}_3/\text{CoFe}_2\text{O}_4$ core-shell composites with excellent electromagnetic absorption performance. *ACS Appl. Mater. Interfaces* 7, 4744–4750. doi: 10.1021/am508438s
- Lv, H., Liang, X., Ji, G., Zhang, H., and Du, Y. (2015b). Porous three-dimensional flower-like Co/CoO and its excellent electromagnetic absorption properties. *ACS Appl. Mater. Interfaces* 7, 9776–9783. doi: 10.1021/acsami.5b01654
- Ning, M. Q., Lu, M. M., Li, J. B., Chen, Z., Dou, Y. K., Wang, C. Z., et al. (2015). Two-dimensional nanosheets of MoS_2 : a promising material with high dielectric properties and microwave absorption performance. *Nanoscale* 7:15734. doi: 10.1039/c5nr04670j
- Qiang, R., Du, Y., Wang, Y., Wang, N., Tian, C., Ma, J., et al. (2016). Rational design of yolk-shell C/C microspheres for the effective enhancement in microwave absorption. *Carbon* 98, 599–606. doi: 10.1016/j.carbon.2015.11.054

Through controlling the reaction temperature and time, products with uniform morphology are obtained. The results reveal that the interesting porous structure of Ni_xS_y might benefit the access of incident microwave and offer more active sites for multiple reflections and scattering, and thereby improve microwave absorbing performance. The minimum RL of -35.6 dB is achieved with a thickness of 2.7 mm at -35.6 dB GHz. The absorption bandwidth with RLs below -10 dB is up to 14.5 GHz when considering thicknesses of 2.0–5.0 mm. Combining the synergistic effect with intrinsic chemical properties and special structures, the Ni_xS_y nanorods are promising for utilization as MA materials in various fields, such as aeroplanes and spacecraft.

AUTHOR CONTRIBUTIONS

ML designed experiments, carried out experiments, analyzed experimental results, and wrote the manuscript. QW, WX, H-YZ, and XD helped experimental result. X-HG gave guidance on the revision of the experimental plan and manuscript. G-SW and S-HD funded experimental topics.

ACKNOWLEDGMENTS

This project was supported by the National Nature Science Foundation of China (No. 51472012), and the Fundamental Research Funds for the Central Universities.

SUPPLEMENTARY MATERIAL

The Supplementary Material for this article can be found online at: <https://www.frontiersin.org/articles/10.3389/fchem.2018.00405/full#supplementary-material>

- Wang, B., Wei, J., Yang, Y., Wang, T., and Li, F. (2011). Investigation on peak frequency of the microwave absorption for carbonyl iron/epoxy resin composite. *J. Magnet. Magnetic Mater.* 323, 1101–1103. doi: 10.1016/j.jmmm.2010.12.028
- Wang, G. S., Wu, Y. Y., Zhang, X. J., Li, Y., Guo, L., and Cao, M. S. (2014). Controllable synthesis of uniform ZnO nanorods and their enhanced dielectric and absorption properties. *J. Mater. Chem. A* 2, 8644–8651. doi: 10.1039/c4ta00485j
- Wang, L., Xing, H., Gao, S., Ji, X., and Shen, Z. (2017). Porous flower-like NiO/graphene composites with superior microwave absorption properties. *J. Mater. Chem. C* 5, 2005–2014. doi: 10.1039/c6tc05179k
- Wang, Y., Chen, D., Yin, X., Xu, P., Wu, F., and He, M. (2015). Hybrid of MoS₂ and reduced graphene oxide: a lightweight and broadband electromagnetic wave absorber. *ACS Appl. Mater. Interfaces* 7, 26226–26234. doi: 10.1021/acsami.5b08410
- Wang, Y., Wang, L., and Wu, H. (2013). Enhanced microwave absorption properties of α -Fe₂O₃-filled ordered mesoporous carbon nanorods. *Materials* 6, 1520–1529. doi: 10.3390/ma6041520
- Xu, W., Pan, Y. F., Wei, W., and Wang, G. S. (2018). Nanocomposites of oriented nickel chains with tunable magnetic properties for high-performance broadband microwave absorption. *ACS Appl. Nano Mater.* 1, 1116–1123. doi: 10.1021/acsanm.7b00293
- Yan, D., Cheng, S., Zhuo, R. F., Chen, J. T., Feng, J. J., Feng, H. T., et al. (2009). Nanoparticles and 3D sponge-like porous networks of manganese oxides and their microwave absorption properties. *Nanotechnology* 20:105706. doi: 10.1088/0957-4484/20/10/105706
- Yang, R., Wang, B., Xiang, J., Mu, C., Zhang, C., Wen, F., et al. (2017). Fabrication of NiCO₂-anchored graphene nanosheets by liquid-phase exfoliation for excellent microwave absorbers. *ACS Appl. Mater. Interfaces* 9, 12673–12679. doi: 10.1021/acsami.6b16144
- Yu, M., Liang, C., Liu, M., Liu, X., Yuan, K., Cao, H., et al. (2014). Yolk-shell Fe₃O₄@ZrO₂ prepared by a tunable polymer surfactant assisted sol-gel method for high temperature stable microwave absorption. *J. Mater. Chem. C* 2, 7275–7283. doi: 10.1039/c4tcQ1285b
- Yuan, K., Che, R., Cao, Q., Sun, Z., Yue, Q., and Deng, Y. (2015). Designed fabrication and characterization of three-dimensionally ordered arrays of core-shell magnetic mesoporous carbon microspheres. *ACS Appl. Mater. Interfaces* 7, 5312–5319. doi: 10.1021/am508683p
- Zhang, C., Wang, B., Xiang, J., Su, C., Mu, C., Wen, F., et al. (2017). Microwave absorption properties of CoS₂ nanocrystals embedded into reduced graphene oxide. *ACS Appl. Mater. Interfaces* 9, 28868–28875. doi: 10.1021/acsami.7b06982
- Zhang, D. D., Zhao, D. L., Zhang, J. M., and Bai, L. Z. (2014). Microwave absorbing property and complex permittivity and permeability of graphene-CdS nanocomposite. *J. Alloys Compounds* 589, 378–383. doi: 10.1016/j.jallcom.2013.11.195
- Zhang, X., Ji, G., Liu, W., Quan, B., Liang, X., Shang, C., et al. (2015). Thermal conversion of an Fe₃O₄@metal-organic framework: a new method for an efficient Fe-Co/nanoporous carbon microwave absorbing material. *Nanoscale* 7, 12932–12942. doi: 10.1039/c5nr03176a
- Zhang, X. J., Wang, S. W., Wang, G. S., Li, Z., Guo, A. P., Zhu, J. Q., et al. (2017). Facile synthesis of NiS₂@MoS₂ core-shell nanospheres for effective enhancement in microwave absorption. *RSC Adv.* 7, 22454–22460. doi: 10.1039/c7ra03260a
- Zhang, Y., Huang, Y., Zhang, T., Chang, H., Xiao, P., Chen, H., et al. (2015). Broadband and tunable high-performance microwave absorption of an ultralight and highly compressible graphene foam. *Adv. Mater.* 27, 2049–2053. doi: 10.1002/adma.201405788
- Zhao, B., Guo, X., Zhao, W., Deng, J., Shao, G., Fan, B., et al. (2016). Yolk-Shell Ni@SnO₂ composites with a designable interspace to improve the electromagnetic wave absorption properties. *ACS Appl. Mater. Interfaces* 8, 28917–28925. doi: 10.1021/acsami.6b10886
- Zhao, B., Shao, G., Fan, B., Zhao, W., Xie, Y., and Zhang, R. (2015). Facile preparation and enhanced microwave absorption properties of core-shell composite spheres composed of Ni cores and TiO₂ shells. *Phys. Chem. Chem. Phys.* 17, 8802–8810. doi: 10.1039/c4cp05632a
- Zhao, H., Li, Z., Zhang, N., Du, Y., Li, S., Shao, L., et al. (2014). γ -irradiation induced one-step synthesis of electromagnetic functionalized reduced graphene oxide-Ni nanocomposites. *RSC Adv.* 4, 30467–30470. doi: 10.1039/c4ra05477f
- Zhao, H. B., Fu, Z. B., Chen, H. B., Zhong, M. L., and Wang, C. Y. (2016). Excellent electromagnetic absorption capability of Ni/Carbon based conductive and magnetic foams synthesized via a green one pot route. *ACS Appl. Mater. Interfaces* 8, 1468–1477. doi: 10.1021/acsami.5b10805
- Zhou, J. H., He, J. P., Li, G. X., Wang, T., Sun, D., Ding, X. C., et al. (2010). Direct incorporation of magnetic constituents within ordered mesoporous carbon-silica nanocomposites for highly efficient electromagnetic wave absorbers. *J. Phys. Chem. C* 114, 7611–7617. doi: 10.1021/jp911030n
- Zhu, C. L., Zhang, M. L., Qiao, Y. J., Xiao, G., Zhang, F., and Chen, Y. J. (2010). Fe₃O₄/TiO₂ core/shell nanotubes: synthesis and magnetic and electromagnetic wave absorption characteristics. *J. Phys. Chem. C* 114, 16229–16235. doi: 10.1021/jp104445m
- Zhu, H. L., Bai, Y. J., Liu, R., Lun, N., Qi, Y. X., Han, F. D., et al. (2011). *In situ* synthesis of one-dimensional MWCNT/SiC porous nanocomposites with excellent microwave absorption properties. *J. Phys. Chem.* 21, 13581–13587. doi: 10.1039/c1jm11747e

Conflict of Interest Statement: The authors declare that the research was conducted in the absence of any commercial or financial relationships that could be construed as a potential conflict of interest.

Copyright © 2018 Lu, Wu, Guan, Xu, Zhang, Di, Wang and Dong. This is an open-access article distributed under the terms of the Creative Commons Attribution License (CC BY). The use, distribution or reproduction in other forums is permitted, provided the original author(s) and the copyright owner(s) are credited and that the original publication in this journal is cited, in accordance with accepted academic practice. No use, distribution or reproduction is permitted which does not comply with these terms.